

DEBRISK V3: NEW GENERATION OF OBJECT-ORIENTED TOOLS

J. Annaloro⁽¹⁾, S. Galera⁽²⁾, C. Thiebaut⁽³⁾, P. Omalý⁽¹⁾

⁽¹⁾ *Orbital Systems Direction, Centre National d'Etudes Spatiales, Toulouse, France, julien.annaloro@cnes.fr*

⁽²⁾ *ALTRAN Sud-Ouest, Toulouse, France*

⁽³⁾ *Launch Vehicle Direction, Centre National d'Etudes Spatiales, Paris, France*

ABSTRACT

Since 2015, improvements in the physical modelling of the re-entry phenomena have been taken into account within DEBRISK, the French certification tool. Lots of activities have been set up in order to understand and finally reduce as much as possible the uncertainties still present in the physical models within this type of tool.

This paper focuses particularly on the development of new aerothermodynamics models within DEBRISK. The impact of these new models, based on Computational Fluid Dynamics (CFD) campaign for the continuous hypersonic regime, is significant on the survivability of the debris.

1 INTRODUCTION

Since 1957 and the launch of Sputnik-1, an amazing quantity of human-made objects have reached Earth orbits. Mitigation is therefore required and de-orbitation is mandatory: at the end of the operational life, Low Earth Orbit (LEO) satellites need to be removed by re-entering the Earth's atmosphere.

However, the atmospheric re-entry of debris could pose significant risks. Debris fragments that survive and reach the surface of the Earth could represent an impact risk to people and property. A number of existing guidelines and regulations in several countries use the probability 10^{-4} as the threshold for the re-entry casualty risk. Specifically, in France where the French Space Operation Act (LOS) was adopted in 2008.

In this context, the French Space Agency (CNES) is in charge of ensuring the right application of the technical regulation introduced in the law by evaluating the prospective risk. In this context, CNES develops its own certification tool, DEBRISK, since 2008. DEBRISK is based on an object-oriented approach. The main idea is to simplify the vehicle geometry into individual simple shapes, available within the software. The trajectory, the thermal heat load and the possible ablation processes are computed with approximate physical models for each fragment. Finally, the demise altitude or the casualty area (in case of survivability) are provided.

Since 2012, a version v2 of the software is provided to space operators, allowing them to independently carry out atmospheric re-entry analysis. Since 2015, a version v3 is in progress [1]. The main objective is to work on the reduction of uncertainties on the models implemented in order to increase our confidence in the results from this kind of tools.

For this paper, we would like to focus particularly on the aerothermodynamics modelling. In the version v3 of DEBRISK, a large aerothermodynamics database has been built for the hypersonic continuum regime, through CFD computations, in order to no longer rely on historical formulations from Klett's work [2]. The impact of these new models is significant on the debris survivability, when a comparison is performed with the Klett's methodology.

The first chapter is devoted to a review of the Klett's methodology by focusing on the simplifying assumptions proposed by the author. The second chapter presents the new methodology of DEBRISK v3, consisting in setting up a CFD numerical database from which aerodynamics and aerothermodynamics models are derived using interpolation schemes. In order to validate this methodology, the following chapter presents experiments carried out in the VKI Longshot hypersonic tunnel using hollow cylinders and hemispherical shells. Aerodynamic coefficients are determined for a wide range of attitudes using a non-intrusive free-flight technique. Heat fluxes are also measured, from which the total power received by the objects is estimated. A comparison is performed, between CFD numerical results with the experimental data obtained, in order to validate the methodology of DEBRISK V3.

2 KLETT'S METHODOLOGY REVIEW

Heat fluxes and drag coefficients formulations used in DEBRISK version 2, are based on the Klett's methodology [2]. This methodology was extremely valuable from the 60's and implemented in most certification tools as ORSAT [4] and SESAM [5]. Historically, this methodology is only applied for right circular cylinder, but it was generalized by others contributors to be applicable to other objects as sphere, box and flat plate [3, 4].

Nowadays, 3D CFD codes are enough advanced to overcome the use of this type of methodology. Thereby, more than 200 CFD computations have been performed in collaboration with R.Tech. Results are provided by the MISTRAL CFD code and are used to investigate the accuracy of these historical formulas.

Table 1 summarizes the result of these comparisons where a large number of dimensions are taken into account (one sphere, three sizes of cylinders, five sizes of boxes/flat plates). Moreover, three realistic trajectory points are chosen (respectively Mach 9, 15 and 20). The results presented are integrated, according to the movement of the shape (Random-tumbling for spheres and cylinders, End-Over-End for the Boxes and Plates). This table shows that the differences obtained are important with a trend which is always the same: with CFD computations, convective heat fluxes are smaller while drag coefficients are higher.

These results show that the use of Klett's methodology for spacecraft demise assessments would underestimate the survivability of debris.

	Drag coefficient	Heat fluxes
Sphere	[-2% +1%]	[-22% -17%]
Cylinder	[+7% +28%]	[-23% -15%]
Box	[-5% +28%]	[-34% -29%]
Plate	[+28% +33%]	[-8% -4%]

Table 1. Relative discrepancies between the MISTRAL calculations and the Klett's methodology.

The most notable differences for the cylinder shape are explained below, by highlighting some assumptions proposed by Klett.

2.1 Drag coefficient

First, the Klett's methodology proposes to estimate drag coefficient for two specific angles of attack: 0° (end-on position facing the flow) and 90° (broadside position facing the flow). Moreover, an empirical bridging function is proposed in order to make the link between these two angles, such as:

$$C_{D\alpha} = C_D^{Broadside} \sin^3 \alpha + C_D^{EndOn} \cos^3 \alpha \quad (1)$$

Hereunder on Figure 1, comparisons between the Klett's methodology and CFD computations (where no assumptions are needed) are performed for 3 geometric ratios of right circular cylinders, at Mach 20. This figure shows that the comparison is quiet consistent for 0° and 90° . The differences are rather at the level of the other angles. Furthermore, when drag coefficient is integrated according to the movement, the differences depend on the length and can reach almost 30%.

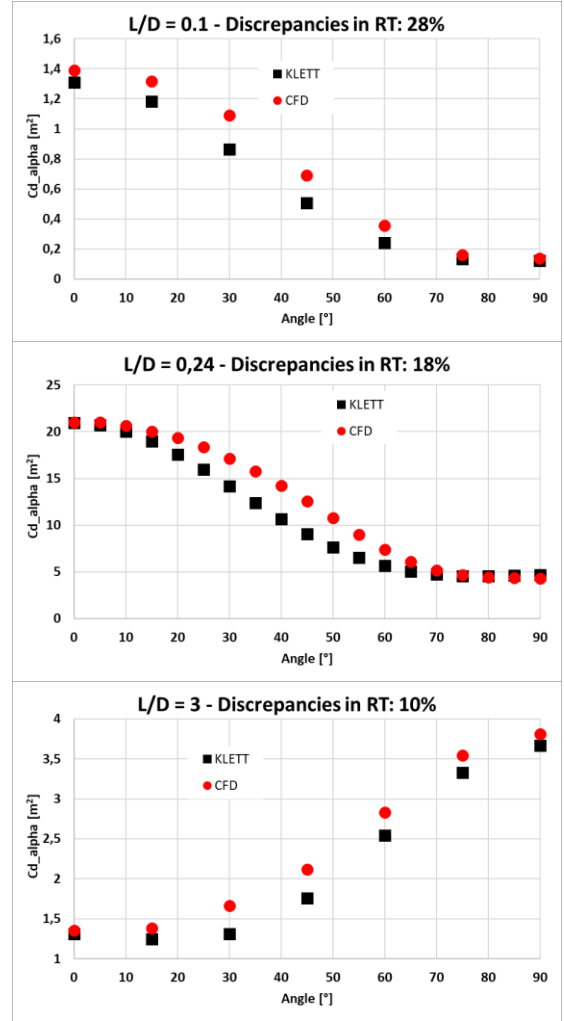


Figure 1. Relative discrepancies of 3D CFD calculations with regard to Klett's methodology, for drag computations over right circular cylinders.

2.2 Convective heat flux

To estimate thermal heat fluxes, the Klett's methodology proposes to rely on a density heat flux at the stagnation point of a sphere (q_{SS}) and multiply it by a sum of shape factors (F_{RT}^{face}), integrated according to the movement, such as:

$$\bar{Q}_{RT}^{Object} = q_{SS} \times (\sum_{faces} F_{RT}^{face}) \times S_{th}^{Object} \quad (2)$$

In the cylinder case, shapes factors are F_{RT}^{EndOn} and $F_{RT}^{Broadside}$, corresponding respectively to the two disc parts and the broadside part, as shown on Figure 2.

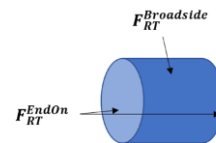


Figure 2. Shape factors on cylinders.

Each of these shape factors is a combination of multiple contributions, independently derived from different experiences.

2.2.1 The end-on part

For the disk part, as shown in Figure 3 and Figure 4, it is important to notice that the shapes tested in the experiment from which Klett relies on, correspond to cylinders with rounded edges and not with right circular edges, as introduced by Klett in [2].

In Figure 3, the black line corresponds to interpolation used by Klett to estimate the heat flux of the right face from 0° to 90°, divided by the heat flux at 0°. This interpolation is derived from experiences (red dotted line) performed on a rounded shape (shown on the right part of picture), and detailed in [6]. Comparisons with CFD computations (colored squares), by taking into account several lengths of cylinders with right circular edges and different Mach numbers, show that the Klett's interpolation overestimates the heat fluxes. Once integrated according to the movement, the difference can reach -30%.

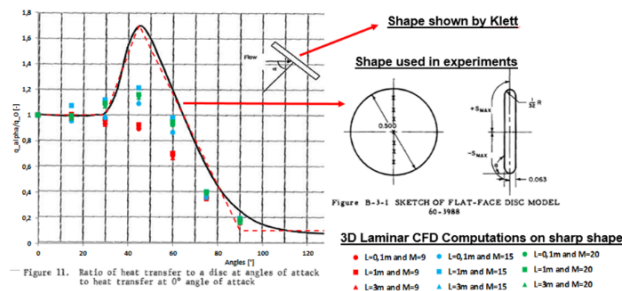


Figure 3. Ratio of heat transfer to the right face at angles of attack to 0° angle value.

Comparison between Klett's interpolation on real shape used, and CFD computations.

In Figure 4, the interpolation proposed by Klett is also in black line. This interpolation estimates the local heat flux distribution on the right face at 0° angles of attack, derived from experiences performed on the rounded shape [7], as well. Comparisons with CFD computations (colored lines) and non-correlated experimental data found in [8] on several cylinders with right circular edges and different Mach numbers, show again that the Klett's interpolation overestimates heat fluxes. In addition, Klett's methodology assumes the same the profile regardless of the length of the cylinder. This assumption is not confirmed by CFD, as it is shown in the figure. Furthermore, CFD computations and experimental data are rather consistent.

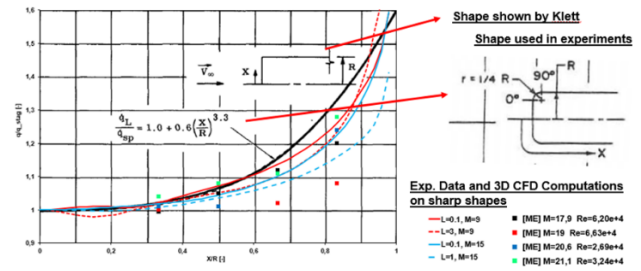


Figure 10. Ratio of local heating to stagnation-point heating on the front end of an end-on cylinder ($\theta = 0^\circ$)

Figure 4. Local heat flux distribution on the right face at 0° angles of attack.

Comparison between Klett's interpolation, CFD computations and experimental data.

2.2.2 The broadside part

Figure 5 presents the broadside part at 90° of angle of attack. As for the end-on part, it is interesting to notice that the shapes tested in the experiment from which Klett relies on, correspond to the hemispherical end cap of a cylinder and not the broadside part, as introduced by Klett in [2].

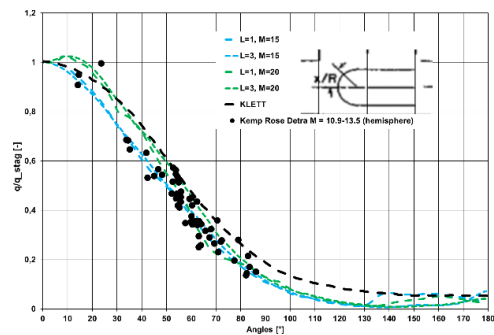


Figure 5. Heat flux distribution on the hemispherical end cap of cylinder.

Comparison between Klett's interpolation, experimental data used by Klett and CFD computations.

In this figure, the dotted black line corresponds to interpolation used by Klett to estimate the local heat transfer distribution on the broadside part of a cylinder at 90° of angle of attack. Comparisons with the experimental data used by Klett (from Kemp, Rose and Detra [7]) and CFD computations (colored dotted lines) on several broadside parts of cylinders and different Mach numbers, show again that the Klett's interpolation overestimates heat fluxes: it is very surprising to note that the proposed interpolation seems to overestimate the experimental data itself. Assuming the following interpolated formula, given by ORSAT in [4], where α corresponds to the angle of attack and θ corresponds to the circumferential angle, the parameter β has been calibrated by ourselves from experimental data of Kemp, Rose and Detra.

$$\frac{q_{\alpha=90^\circ, \theta}^{Broadside}}{q_{\alpha=90^\circ, \theta=0^\circ}^{Broadside}} = \cos\left(\frac{\theta}{2}\right)^\beta \quad (2)$$

Once the interpolation recalibrated and integrated according to θ , the difference is about -16% between the interpolation from Klett and our interpolation.

Last comment already highlighted in the previous section: one of the main assumption of the Klett's methodology is that 3D effects are not taken into account. The profile proposed by Klett is always the same whatever the length of the cylinder. This assumption is not confirmed by CFD computations, as show in Figure 6, especially when the length of the cylinder is smaller than the diameter.

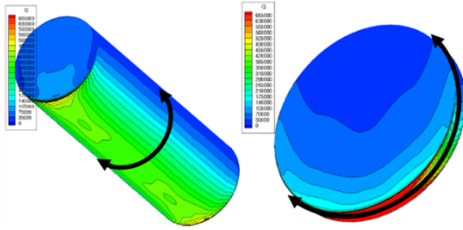


Figure 6. CFD computations of heat transfer distribution on a cylinder at 90° of angle of attack, at Mach 20.

2.3 Application case

In this section, we would like to challenge the Klett's methodology by testing it on a cylinder with hemispherical edges, using CFD computations. This methodology can be used to build the drag coefficient and the heat flux of a hemispherical cylinder, assuming the following equations:

$$C_{D,RT}^{Hem} S_{Aero}^{Hem} = C_{D,RT}^{Broadside} S_{Aero}^{Broadside} + C_{D,RT}^{Sphere} S_{Aero}^{Sphere} \quad (3)$$

$$q_{RT}^{Hem} S_{Th}^{Hem} = q_{RT}^{Broadside} S_{Th}^{Broadside} + q_{RT}^{Sphere} S_{Th}^{Sphere} \quad (4)$$

where exponents "Hem" and "Broadside" means, respectively, "Hemispherical cylinder", and "Broadside part" of a right circular cylinder. The subscript "RT" means integrated according to random tumbling movement. For our test-case, the data used in the right hand side of equations come from two independent CFD calculations.

Figure 7 and Figure 8 show for different angles of attack, CFD computations comparisons between such a reconstruction (equation (4)) and a hemispherical cylinder (without assumptions). Integrated according to the movement, and combined following the previous equations, more than 20% of discrepancy is observed for the thermal flux. This comparison shows that the Klett's methodology is not perfectly suitable to the reconstruction of new shapes.

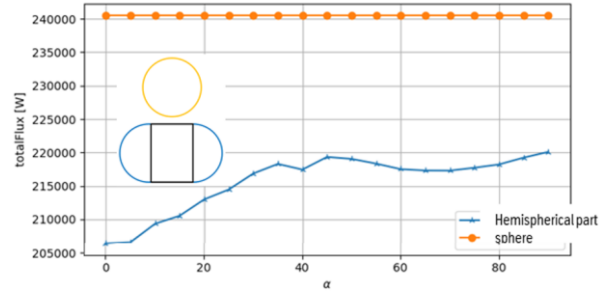


Figure 7. Heat flux computed on a sphere (orange line) and on the two hemispherical part of a cylinder (blue line). CFD computations at Mach 9.

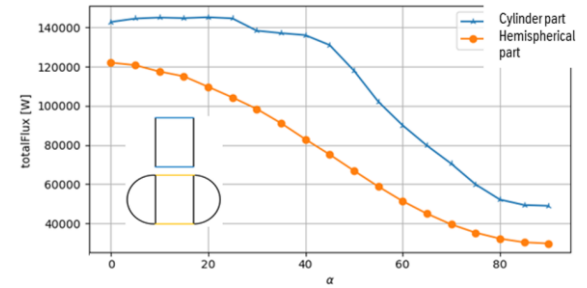


Figure 8. Heat flux computed on the broadside of a right circular cylinder (blue line) and on the broadside part of a hemispherical cylinder (orange line). CFD computations at Mach 9.

2.4 Conclusions

Globally, engineering formula from the 60's, on classical shapes underestimate the drag coefficient and overestimate the integrated heat flux. It is important to keep in mind that the use of such methodology for spacecraft demise assessments would underestimate the survivability of debris.

Besides the fact that Klett does not always use the right shape of cylinders to determine heat fluxes, and overestimate experimental data found in the literature, this methodology, which is used for all classical shapes, relies on strong assumptions, as:

- Bridging function to calculate the drag coefficient,
- Face by face combination from independent data contribution,
- No consideration of 3D effects and geometric ratio dependency,
- Extrapolation of cylinder interpolations to sphere, box and plate (ORSAT [4]).

Conversely, CFD computations are free from these assumptions. Therefore, an aerothermodynamics database built from CFD calculations is recommended to be more realistic.

3 NEW AEROTHERMODYNAMICS DATABASE

3.1 Shapes available in DEBRISK

Five simple topologies are introduced in DEBRISK (cf. Table 2): spheres, straight edge cylinders, hemispherical cylinders, boxes and flat plates. Moreover, six new topologies are added (Table 3) : open cylinders, open truncated cones, spherical caps as well as the angular sectors of these three shapes.

The survivability analysis of any debris shapes, requires to compute along the entire trajectory, the drag force and the convective heat flux. DEBRISK v3 now allows to determine these two quantities of interest via a CFD database in continuum hypersonic regime. This database is built to be applicable whatever the Mach number and the dimensional changes of the topologies mentioned above. The drag coefficients and the convective heat fluxes are derived using interpolations schemes. More details on how to build this database can be found in [9].

Table 2. Simple shapes implemented within DEBRISK

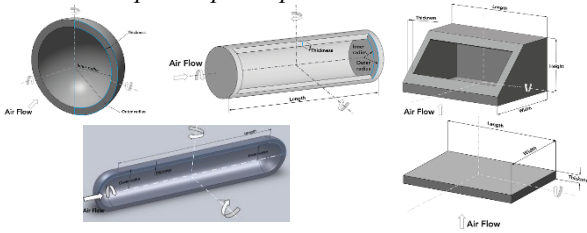
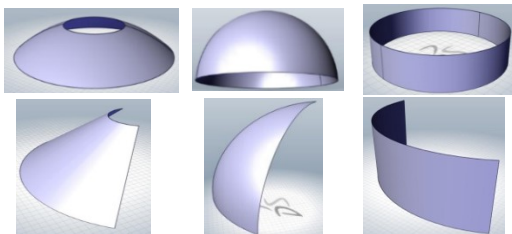


Table 3. Complex shapes implemented within DEBRISK



3.2 Methodology for CFD computations

For each shape, the attitude is assumed to be in a random tumbling movement (except for boxes and flat plates where an End-over-End movement is applied). A methodology is therefore developed to take into account this specific movement. The CFD computation campaign is performed using an innovative method: the purpose is to reduce time-consuming step of the mesh generation for each attitude. The method is based on the creation of a single coarse mesh, which is called “rotating mesh”, (see Figure 9, Figure 10 and Figure 11).

Through this unique mesh, a large number of simulation points of view (attitude) are placed in a uniform way as shown in Figure 12. Each point of view corresponds to a CFD simulation with the MISTRAL software for a single direction (attitude) of flow. This approach eliminates the multiple mesh generations (one for each attitude) while maintaining the accuracy. About 3000 CFD computations were performed via this methodology in order to feed the aerothermodynamics database.

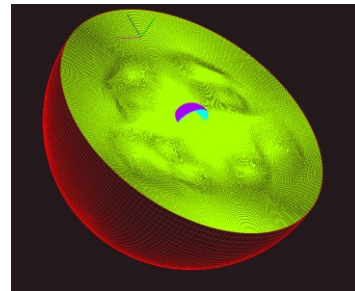


Figure 9. Spherical inflow/outflow domain

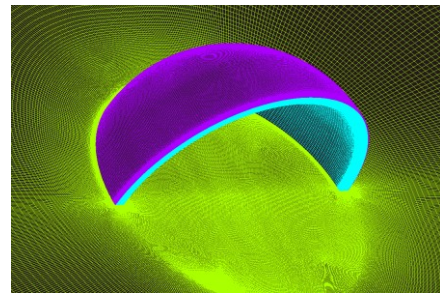


Figure 10. High density mesh around hollow hemisphere

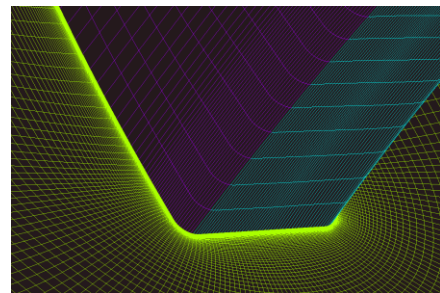


Figure 11. Close up around corners of hollow hemisphere

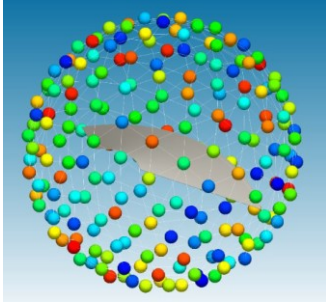


Figure 12. Distribution of simulation points of view

4 EXPERIMENTAL INVESTIGATIONS

4.1 Objectives

The purpose of this hypersonic experiments campaign is to determine the drag coefficients and the total convective heat fluxes for two specific geometries, in order to validate the numerical results obtained with the rotating mesh approach described in §3.2. This comparison has been the subject of two publications [9, 9]. The following sections summarize its publications.

4.2 The VKI Longshot hypersonic gun tunnel

The VKI Longshot facility illustrated in Figure 13 is a hypersonic gun tunnel operated at the von Karman Institute for Fluid Dynamics, in Belgium. It is established as a reference European facility for aerothermodynamics investigations in low-enthalpy perfect gas environments. This wind tunnel is able to generate flows at high Mach numbers (Mach 10-20) together with the large Reynolds numbers pertaining to most of Earth reentry trajectories, including the ones followed by space debris.

This wind tunnel benefits from state-of-the-art flow characterization methods detailed in [11] and is therefore particularly well-suited for the present validation of a novel numerical approach.

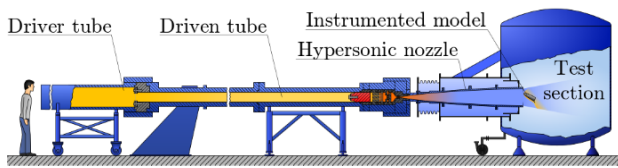


Figure 13. Sketch of the VKI Longshot hypersonic tunnel.

4.3 Geometries selected for wind tunnel experiments

Geometries of interest were identified based on the specific flow features they would exhibit for some re-entry attitudes. Attached shock waves, shock-shock interactions, shock-boundary layer interactions, flows over concave surfaces, or unsteady flows configurations

were deemed particularly interesting to challenge the numerical code.

Two geometries have been selected for the experimental investigations: a hollow hemisphere (typically representing a propellant reservoir split in two), and an annular ring with an aspect ratio of 1/4th (corresponding to a rocket interstage fairing). Both geometries are illustrated in Figure 14. They present the different flow features of interest.

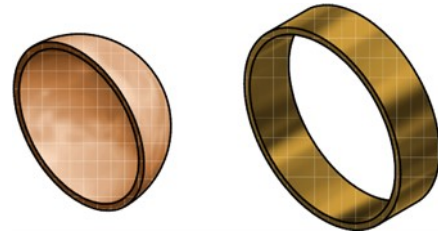


Figure 14. Scaled models (hollow hemisphere and annular ring) tested in the VKI Longshot tunnel.

4.4 Test matrices

A total number of 31 experiments are performed in the VKI Longshot tunnel using a contoured nozzle with an exit diameter of 426mm. It provides a uniform flow field at Mach 11 with a useful test time on the order of 20ms. Pure nitrogen is used as a test gas for the present experiments which prevents the onset of chemical reactions given the moderate specific stagnation enthalpies which are involved (<3MJ/kg).

Longshot operating conditions are selected in order to match both Mach and Reynolds numbers (two major similarity parameters for aerothermodynamics investigations) as experienced by space debris during their re-entries, as illustrated in Figure 15.

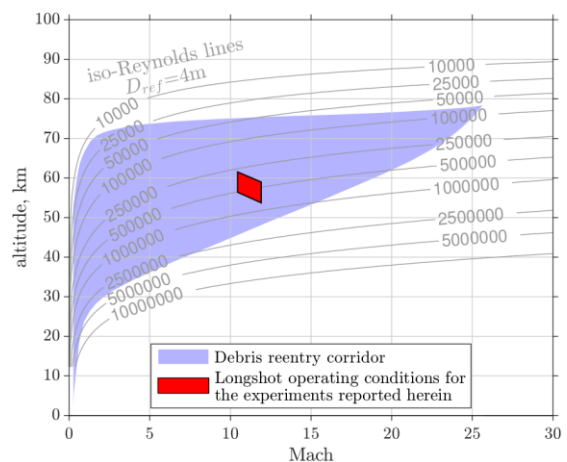


Figure 15. Re-entry corridor for space debris and selected Longshot flow conditions for the present experiments

15 Longshot runs are dedicated to aerodynamic investigations using the free-flight measurement technique. The next 16 Longshot runs are performed on the same geometries, but fixed within the test section, and equipped with instrumentation. They include 15 fast-response coaxial thermocouples from which the local wall heat fluxes are determined. 15 pressure sensors are also distributed over each model. The thermocouples and pressure sensor have been placed at locations where the most complex flow physics is expected (based on preliminary numerical computations) (see Figure 16).

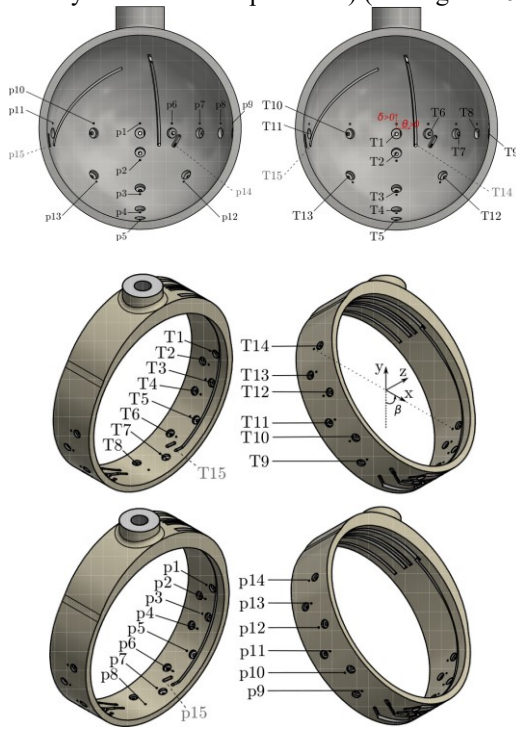


Figure 16. Instrumented locations

4.5 Validation of the DEBRISK V3 methodology

Both the free flight experiments and the instrumented experiments have been rebuilt via MISTRAL, by using the same methodology presented in section 3.2. The variations in angle of attack are performed in steps of 5 degrees. For the hollow sphere the angles range from -90° to 90° , while for the annular ring the angles span from 0° to 90° . The angle of attack for these models is defined from Figure 17.

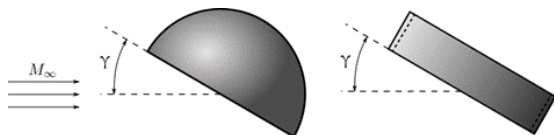


Figure 17. Convention used for the angle of attack

4.5.1 Drag coefficient

Experimental data obtained in the VKI Longshot tunnel

for the hypersonic aerodynamics of a hemisphere are presented in Figure 18, using thick black lines. Free-flight models are successively released at different angles of attack and are then free to adjust to new attitudes depending on the aerodynamic forces which are exerted on them. This enables to cover a wide range of attitudes using only a few experimental runs.

Numerical predictions are in good agreement with experimental results, including also the attitudes ($25^\circ < \gamma < 60^\circ$) for which unsteady flows are present over the hemispherical model as it exposes its concave surface to the incoming flow. The individual angles have been integrated in order to obtain the random tumbling averaged drag coefficient (see Table 4). The numerical value corresponds almost perfectly to the experimental value for the hollow sphere.

Table 4. Averaged drag coefficient for the hollow hemisphere

$C_{d_{avg}}$	
Experimental value	0.762
Numerical value	0.744
Discrepancy (%)	2.5

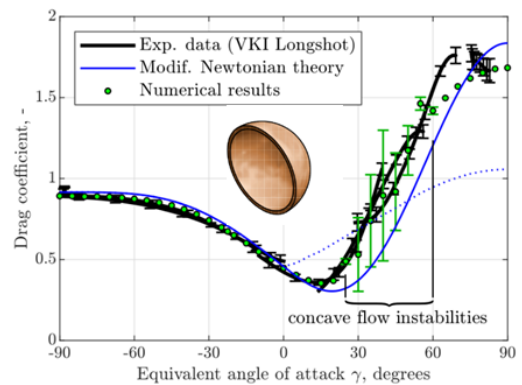


Figure 18. Drag coefficient for a hypersonic hollow hemisphere for different angles of attack.

Similar results are presented for the annular ring in Figure 19. This geometry is much more stable than the previous one and free-flight experiments with angles of attack beyond 25° could only be covered for rather discrete values. The numerical predictions are again in very good agreement with the experiments which indicates that the pressure distribution along the different objects is predicted correctly. The individual angles have been integrated in order to obtain the random tumbling averaged drag coefficient (see Table 5). As for the hollow sphere, an excellent agreement between the numerical value and the experimental value is obtained for the annular ring

Table 5. Averaged drag coefficient for the annular ring

$C_{d,avg}$	
Experimental value	1.664
Numerical value	1.626
Discrepancy (%)	-2.3

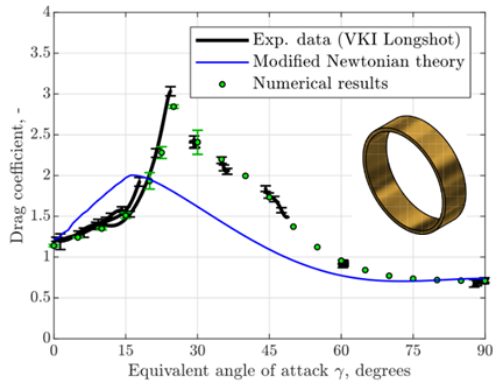


Figure 19. Drag coefficient for a hypersonic annular ring for different angles of attack.

4.5.2 Convective heat fluxes

The methodology to compute the total power on shapes, is direct via the CFD results (the results are integrated over on whole object and on all angles of attack). However, from the experimental point of view, assumptions must necessarily be set up to access this quantity via the discrete measurement points (which therefore do not cover the whole object). The total power given by the experiment is therefore not as precise as the uncertainty given by measuring instruments.

Figure 20 compares the total power calculated directly by MISTRAL (orange and blue curves) with the assessment made from the experimental data of the VKI (green curve). We first observe a good convergence between the coarse and average mesh for the stable angles ($[-90^\circ, +30^\circ]$ and $[+60^\circ, +90^\circ]$) and a very good correlation with the experimental data. For the range $[+30^\circ, +60^\circ]$, significant instabilities are observed, which results in large amplitudes around the average value obtained by the stationary CFD calculations. These instabilities are explained by the unsteady nature of the flow.

Finally,

Table 6 presents the average total power obtained for a random-tumbling attitude (quantity of interest for DEBRISK). The agreement is excellent as the discrepancy between CFD and experience is less than 9%.

Figure 21 compares the total power for the annular ring. We note a good agreement between the result, apart from the peak at the specific angle of 22.5° , where strong instabilities were observed, both on the CFD and experiment side. Table 7 shows the mean total power

obtained for a random-tumbling attitude. The agreement is once again excellent as the discrepancy between the CFD computations and experiments is less than 2%.

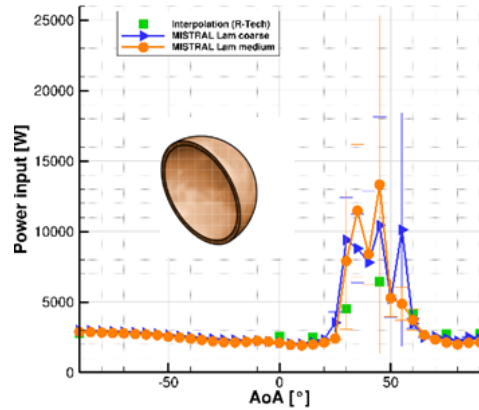


Figure 20. Total power (W) for a hypersonic hollow hemisphere for different angles of attack.

Table 6. Averaged total power for the hollow hemisphere

Q (W)	
Experimental value	3262
Numerical value (medium mesh)	3540
Discrepancy (%)	8.5

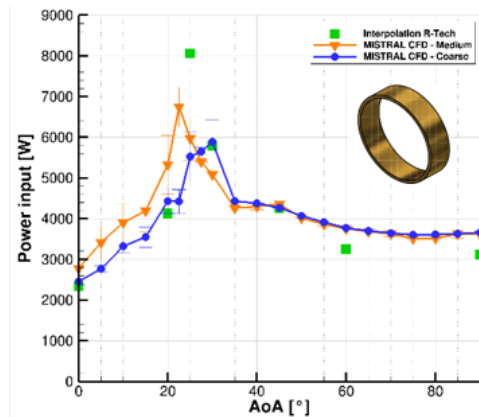


Figure 21. Total power (W) for a hypersonic annular ring for different angles of attack.

Table 7. Averaged total power for the annular ring

Q (W)	
Experimental value	4211
Numerical value (medium mesh)	4281
Discrepancy (%)	1.7

5 CONCLUSIONS

A new methodology is implemented in DEBRISK V3 for the aerothermodynamics modelling, based on a CFD database being able to deal with a large variety of topologies. This methodology is validated by setting up an aerothermodynamics experimental campaign, where a good agreement is observed, as well as for the drag

coefficient and the convective heat flux: less than 3% and 8% of discrepancies, respectively.

Through this paper, we also wanted to compare our new methodology with the one proposed by Klett in the 60's: We have shown that the Klett's methodology is based on strong assumptions and can lead to underestimating the risk on the ground.

6 REFERENCES

1. Omalý P., Annaloro J. (2019). DEBRISK v3: CNES tool evolutions for re-entry risk analysis. *10th International association for the advancement of space safety conference, 15-17 May 2019, Los Angeles (USA)*
2. Klett, R. (1964). Drag Coefficients and Heating Ratios for Right Circular Cylinders in Free Molecular and Continuum Flow from Mach 10 to 30. *D.SC-RR-64-2141, Sandia Corporation, Dec. 1964*
3. Cropp, L. O. (1965). Analytical Methods Used In Predicting The Re-Entry Ablation Of Spherical and Cylindrical Bodies. *Aerospace Nuclear Safety, SC-RR-65-187, September 1965.*
4. Object Reentry Survival Analysis Tool (ORSAT) – Version 6.0. and its application to spacecraft entry. *IAC-05-B6.3.06.*
5. DRAMA Final Report - Upgrade of DRAMA's Space Entry Survival Analysis Codes (2019). *ESA Contract No. 4000115057/15/D/S, ILR/DRAMA/FR. DUP-FR, Revision: 1.0.2, December 20, 2019. <https://sdup.esoc.esa.int/web/csdtf/home>.*
6. Investigation of re-entry destruction of nuclear auxiliary powerplant (1961). *Research and Advanced Development Division. AVCO Corporation. October 1961.*
7. Kemp, N., H., Rose, P., H., Detra, R., W. (1959). Laminar Heat Transfer Around Blunt Bodies in Dissociated Air. *Journal of the Aerospace Sciences, Vol. 26, No. 7 (1959), pp. 421-430.*
8. Matthews, R. K. and Eaves, Jr., R. H., (1967). Comparison of Theoretical and Experimental Pressure and Heat-Transfer Distributions on Three Blunt Nosed Cylinders in Hypersonic Flow. *AEDC, AEDC-TR-67-148, 1967.*
9. Annaloro J. et al. Aerothermodynamics modelling of complex shapes in the DEBRISK atmospheric re-entry tool: methodology and validation. *Acta Astronautica 171, 388-402.*
10. Grossir, G. et al. Aerodynamic characterization of space debris in the VKI Longshot hypersonic tunnel using a free-flight measurement technique, *Experiments in Fluids 61 (7), 1-13*
11. Grossir G. et al. High temperature and thermal non-equilibrium effects on the determination of free-stream flow properties in hypersonic wind tunnels, *Physics of Fluids, 2018, 30, 126102, 1-13.*